Modeling the basin of attraction as a two-dimensional manifold from experimental data: Applications to balance in humans

Maria S. Zakynthinaki,[1] James R. Stirling,[2] Carlos A. Cordente Martínez,[2] Alfonso López Díaz de Durana,[2] Manuel Sillero Quintana,[2] Gabriel Rodríguez Romo,[2] and Javier Sampedro Molinuevo[2]

[1]*Instituto de Ciencias Matemáticas, CSIC-UAM-UC3M-UCM, c/Serrano 121, 28006 Madrid, Spain*

[2]*Facultad de Ciencias de la Actividad Física y del Deporte. Universidad Politécnica de Madrid. Avda. Martín Fierro 7, 28040 Madrid, Spain*

We present a method of modeling the basin of attraction as a three-dimensional function describing a two-dimensional manifold on which the dynamics of the system evolves from experimental time series data. Our method is based on the density of the data set and uses numerical optimization and data modeling tools. We also show how to obtain analytic curves that describe both the contours and the boundary of the basin. Our method is applied to the problem of regaining balance after perturbation from quiet vertical stance using data of an elite athlete. Our method goes beyond the statistical description of the experimental data, providing a function that describes the shape of the basin of attraction. To test its robustness, our method has also been applied to two different data sets of a second subject and no significant differences were found between the contours of the calculated basin of attraction for the different data sets. The proposed method has many uses in a wide variety of areas, not just human balance for which there are many applications in medicine, rehabilitation, and sport.

Estimating the geometry of the basin of attraction of a nonlinear dynamical system from raw data is a fundamental and challenging problem from both a theoretical and applied point of view. In the present work we obtain a three-dimensional function describing the geometry of the basin of attraction from experimental human balance data. The basin of attraction corresponds to the set of correctable angles that a particular subject can lean to and reverse the motion so as to regain vertical upright stance. The importance of the present study is due to the many diverse experimental applications in which one or more basins of attraction are observed. As a result a method of obtaining a function describing the shape of the basin of attraction and its contours and depth from experimental data is of much use. Regarding the application, human balance is an area which is fundamental to medicine, rehabilitation, and also sport: training, rehabilitation, and injury result in changes in the shape and size of the basin of attraction.[1–3] As a result a method that allows one to detect and track these changes will have many important uses.

I. INTRODUCTION

Recently there has been much interest on bipedal locomotion from the point of view of dynamical systems (see, for example, the focus issue,[4] which includes a number of studies regarding human balance[5,6]). Modeling and analyzing the balance of the human body is a difficult task as the human body is a complex multijoint system that has the possibility for a variety of possible dynamics across different joints and body parts.[7,8] For an extended review on dynamics of human postural transitions, see Ref. 9.

The difficult task of understanding such a complex system as the human body is greatly facilitated, when possible, by reducing the dimensionality of the system under study.[7,10–12] Given a sufficiently small perturbation the human body has the ability to regain balance, following a highly complicated path back to the position of quiet upright stance (see also Refs. 1, 5, and 6). The dynamic response of the postural system to a weak mechanical perturbation can be predicted from the fluctuations exhibited by the system under quasistatic conditions[13] (and thus the human postural control system follows the fluctuation-dissipation theorem). It is therefore possible[13] that the postural control system utilizes the same control mechanisms under quiet-standing and dynamic conditions.

In quiet upright stance, balance, however, does not imply motionless stability: the body oscillates spontaneously and continuously at low amplitude in both the mediolateral and the anteroposterior directions (there is a possibility of making predictions regarding an individual's dynamic response to a mild perturbation using quiet-stance data, regardless of age[14]). This phenomenon of constant displacement and correction of the position of the center of gravity is known as postural sway.[5,7,15,16] Postural sway is indistinguishable from correlated noise[17] and that it can be modeled as a system of bounded, correlated random walks.

In the present work, however, as the perturbation away from the vertical position is of orders of magnitude greater than the motion due to body sway during quiet stance, we

model only the large-scale features of the movement pattern, see also Refs. 1–3. The process of regaining balance is represented in our model as movement within a basin of attraction containing the attractor that corresponds to vertical quiet stance. We show how to obtain this basin of attraction, as a two-dimensional manifold which exists in three dimensions, that corresponds to experimental data of a subject. This function can be used to show asymmetries and differences in the range of movement on different sides of the body. The basin of attraction that models the region in our model,[1] in which such a subject can maintain balance, is of course in general expected to be nonsymmetric. It is worth noticing here that static stability regions with respect to ankle and hip joints were proposed in Ref. 18, while Ref. 19 used a concept based on the mechanical limit of upright stance with respect to the angles of the ankle and the hip, which they called stability cone.

The present study (see also Refs. 1 and 3) considers that the process of regaining balance can be reduced to movement on a two-dimensional phase space of two angles θ_x and θ_y. Given the three components of the ground reaction force F_x, F_y, and F_z, the angle θ_x is defined as the angle between F_x and F_z, while θ_y is defined as the angle between F_y and F_z. This way θ_x gives the angle that the body leans away from the vertical in the anteroposterior (x) direction and θ_y gives the angle that the body leans away from the vertical in the mediolateral (y) direction.

Due to the spiraling back onto the fixed point corresponding to vertical stance ($\theta_x=0$, $\theta_y=0$), this point is modeled as a complex sink.[1] It is also assumed that failure to regain balance leads to the body falling to the floor, a condition the end point of which corresponds to the circle $\theta_x^2+\theta_y^2=\pi/2$.[1,3] Both the point (0,0) and the circle $\theta_x^2+\theta_y^2=\pi/2$ are considered to be attracting states in the phase space of the angles θ_x and θ_y. As explained in Refs. 1 and 3 there exists a set of critical angles θ_x^c and θ_y^c such that for values of $0\le\theta_x\le\theta_x^c$ and $0\le\theta_y\le\theta_y^c$ the subject is able to regain an upright stance, while for values of $\theta_x^c<\theta_x\le\pi/2$ and $\theta_y^c<\theta_y\le\pi/2$ the subject loses balance and (in a theoretical experiment) ends up lying on the floor. The critical angles define a "critical curve," which is repelling and serves as the boundary between the two ultimately different body positions, the upright stance versus horizontally lying on the floor. Viewed from this point of view, the critical curve is the boundary between the two basins of attraction that contain either vertical stance or horizontal failure solutions.

The model[1,3] describes the motion of the body's center of gravity using the following set of coupled ordinary differential equations:

$$\dot{\theta}_x=-f_{ax}(\theta_x,\theta_y)\ f_c(\theta_x,\theta_y)\ f_f(\theta_x,\theta_y), \tag{1}$$

$$\dot{\theta}_y=-f_{ay}(\theta_x,\theta_y)\ f_c(\theta_x,\theta_y)\ f_f(\theta_x,\theta_y), \tag{2}$$

where the functions $f_{ax}(\theta_x,\theta_y)$ and $f_{ay}(\theta_x,\theta_y)$ control the attracting fixed point of the vertical state, the function $f_c(\theta_x,\theta_y)$ models the repelling critical curve, and the function $f_f(\theta_x,\theta_y)$ models the horizontal failure state (attracting circle).

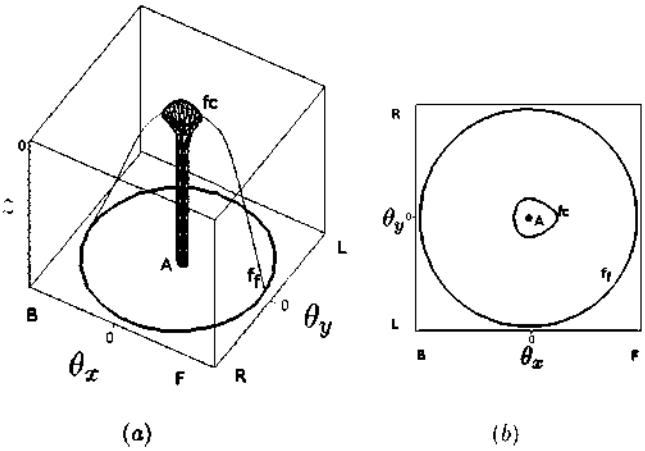

FIG. 1. Idealized features of the model showing the two attracting solutions [point A at (0,0) corresponding to vertical stance and attracting circle of fixed points $f_f(\theta_x,\theta_y)$ that models the horizontal failure state] and the critical curve $f_c(\theta_x,\theta_y)$ that separates their basins of attraction. (a) Three-dimensional representation of the idealized features showing also the basins of attraction. (b) Two-dimensional projection on the phase space of θ_x, θ_y. The letters F, B, R, and L correspond to the four principal directions (forward, backward, right, and left, respectively).

Figure 1 presents the features of the model in a three-dimensional space (θ_x,θ_y,z), where the variable z corresponds to the depth of the two respective potential wells (strength of the attractors). The figure represents an idealized case where the subject's body is symmetrical and therefore a symmetrical critical curve encloses a symmetrical basin of attraction for the spiral sink of (0,0). In the idealized example illustrated in Fig. 1, the subjects' body can lean further toward the positive x-direction and the critical curve is symmetrical regarding the θ_y axis. In Fig. 1, the two attracting features, the point at (0,0) and the circle of radius $\pi/2$, have the same strength, as they are located at equal depths in the z axis.

In reality, however, the process of regaining balance depends on the morphology of the body, the subject's muscular strength, as well as their neurological condition and other factors. When dealing with experimental data, the size and shape of the basin of attraction and the critical curve enclosing it, as well as the strength of the attractor at (0,0), will therefore depend on the individual subject and their condition.

The problem of estimating the basin of attraction of nonlinear dynamical systems is interesting and challenging both from a theoretical and applied point of view. Analytical methods of estimating the basin of attraction of a dynamical system have been developed; however, these methods are obviously limited to dynamical systems that are described by known and analytically manageable functional forms, see, for example, Ref. 20. Basins of attraction are typically studied using initial condition maps which are derived from Poincaré sections, but these are usually limited to two-dimensional surfaces of sections.[21] Some analytical methods arise from the Lyapunov theory of stability,[22–26] while other methods, such as the linearization approach[27] or the so-called tracking function method,[28,29] have been also proposed. Numerical procedures have also been proposed for the calcula-

tion of the basin boundaries from first principles.[30,31] The authors in Ref. 22 suggest the so-called trajectory reversing method that is based on suitable topological considerations. For an extended review on analytical methods for finding the basin of attraction, see Ref. 22.

From the point of view of applications a number of studies have been made in the engineering field (magnetic fields, electric power systems, chemical reactors, and robotics) as well as in other areas such as ecology, biology, and economics.[22] In such studies the basin of attraction (which, in many of these studies, is called the potential well) is estimated numerically through experimental measurements of the potential field (for examples, see Refs. 32–34). In the field of robotics, methods for deriving the equations of motion and impact equations for the analysis of multibody systems, such as walking models,[35] have been investigated. In such models the basin of attraction of the system is estimated by methods such as the so-called cell mapping method.[35] In general, in the field of applications, researchers that study basins of attractions are concerned with the determination of the basin's lower/upper limits or its boundaries (see Ref. 36 as an example).

An interesting method for numerically determining the basin of attraction from experimental data can be found in Ref. 21. In a driven two-well magnetomechanical oscillator, the basins of attractions for the system are obtained using an ensemble of initial conditions that is generated by switching between stochastic and deterministic excitations. Using this so-called stochastic interrogation method, the authors in Ref. 21 demonstrate how to construct transition probability matrices for finite partitions of the phase space. These matrices allow the study of the evolution of probability densities and the estimation of the basins of attraction.

In the present work, the basin of attraction of the system that is described by the model of Ref. 1 is estimated from modeling experimental data (see Sec. II). As will be described in detail in Sec. IV, the method starts in a very similar way to the method described in Ref. 21: the phase space of the system under study is partitioned into an $N \times N$ grid and the number of data points that are contained within each one of the N^2 boxes is counted. The density distribution of the experimental data set is represented as contours on planes parallel to the phase space of the system and is modeled using a family of functions that contain sinusoidals and their harmonics, so as to provide full control of the shape of these contours. The dependence on depth z is modeled using a family of Gaussian functions. The modeling process is such that the curves which the model consists of always provide best fit for the experimental data. The method we propose has been tested here for its robustness and sensitivity to different data sets (please refer to Sec. VII).

For a detailed description of the method, see Sec. IV below.

II. EXPERIMENTAL DATA COLLECTION

A. Experimental procedure

A 25-year old healthy male decathlete of international level served as a subject[37] and a Kistler 9286AA force platform was used, together with its corresponding software for the recording of the ground reaction forces. For the collection of experimental data the following procedure was used, see also Refs. 1, 3, and 37:

FIG. 2. Initial quiet stance: (a) protocol 1 and (b) protocol 2.

- Protocol 1:

(a) The subject initially stood on a force platform with both feet on the floor together and aligned to the anteroposterior axis with hands on hips, see Fig. 2(a). The hands were to remain on the hips throughout the whole experiment.
(b) The subject leaned as far and as fast as he could away from the vertical in all eight directions: forward, backward, left, right, and the four diagonals forward-left, forward-right, backward-left, and backward-right.
(c) A successful data set consisted of the subject being able to correct the perturbation and regain balance in upright stance.

- Protocol 2:

(a) The subject initially stood on a force platform on one leg (first the left and then the right leg), aligned to the anteroposterior axis with hands on hips, with the toes of the other leg touching the ankle of the supporting leg, see Fig. 2(b). The hands were to remain on the hips throughout the whole experiment.
(b) The subject leaned as far and as fast as he could away from the vertical in all eight directions (see protocol 1).
(c) A successful data set consisted of the subject being able

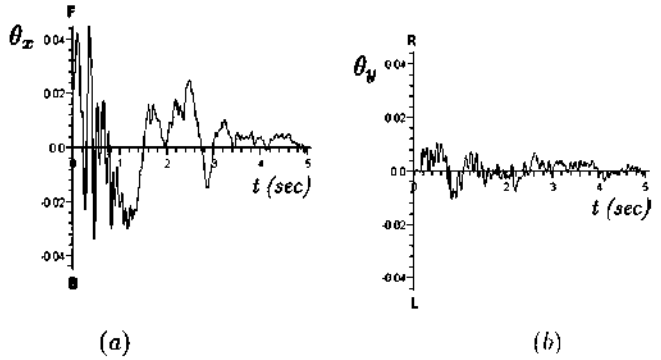

FIG. 3. Example of the time series corresponding to protocol 1 (two-legged stance) and initial perturbation forward: (a) θ_x and (b) θ_y. The letters F, B, R, and L correspond to the four principal directions (forward, backward, right, and left, respectively).

to correct the perturbation and regain balance in an upright stance.

B. Experimental time series data

The time series of the ground reaction force exerted on the ground by the athlete's body were recorded for five successful data sets for each protocol and each of the eight directions (a total of 40 time series data for each posture). The sampling rate was 200 Hz and the total time of each recording was 5 s. Figure 3 shows a characteristic example of the time series of the two angles θ_x and θ_y (these time series correspond to the two-legged stance of protocol 1 and the subject was asked to first lean as far as he could forward). The switch from perturbed stance control to quiet stance control is evident, especially in the time series of Fig. 3(a) that correspond to θ_x, the angle between the vertical and the force exerted by the subject in the anteroposterior direction. The low-scale oscillations present at the end of the recording are quiet stance oscillations.

Figures 4(a)–4(d) show examples of the phase space of the time series of the two angles. These figures correspond to protocol 1, while the subject was asked to lean, on two-legged stance, forward, backward, to the left, and to the right [Figs. 4(a)–4(d), respectively].

Finally, Figs. 5(a)–5(c) present the full set of the 40 experimentally recorded time series for the left-legged, right-legged, and two-legged stance, respectively, plotted in the phase space of the angles (θ_x, θ_y). In these plots the presence of oscillations, as the body is trying to regain balance, is obvious: the more unstable the body the larger the oscillation. During a successful restoration of balance, these oscillations die out as the body regains balance and is back onto the attractor (0,0) that corresponds to the vertical position.

III. NUMERICAL CALCULATION OF THE MODEL'S FEATURES

A. Fitting the model curves to the experimental data

In Secs. II A and IV–VI we will describe how the basin of attraction of our model can be estimated step by step. First we obtain the critical curve that corresponds to a particular

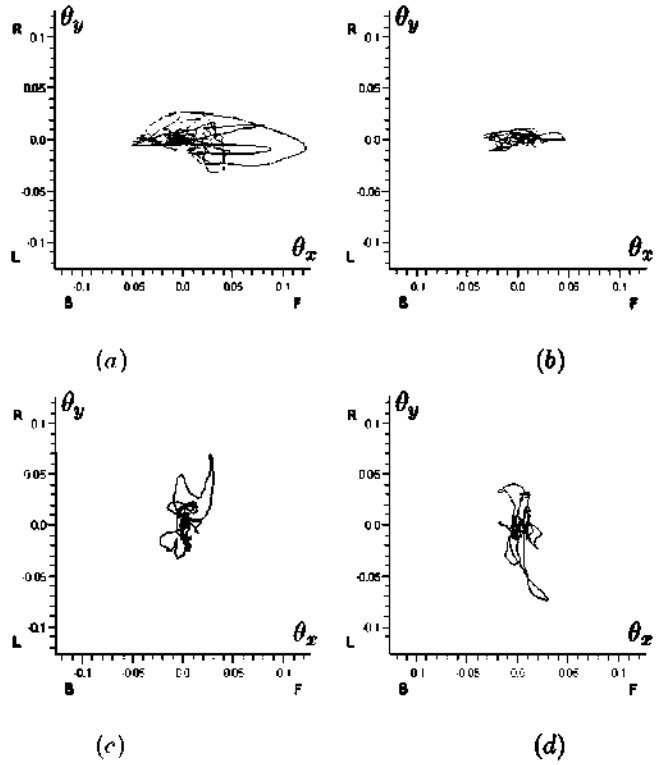

FIG. 4. Examples of the phase space corresponding to protocol 1 (two-legged stance). The subject was asked to lean (a) forward, (b) backward, (c) to the left, and (d) to the right. The letters F, B, R, and L correspond to the four principal directions (forward, backward, right, and left, respectively).

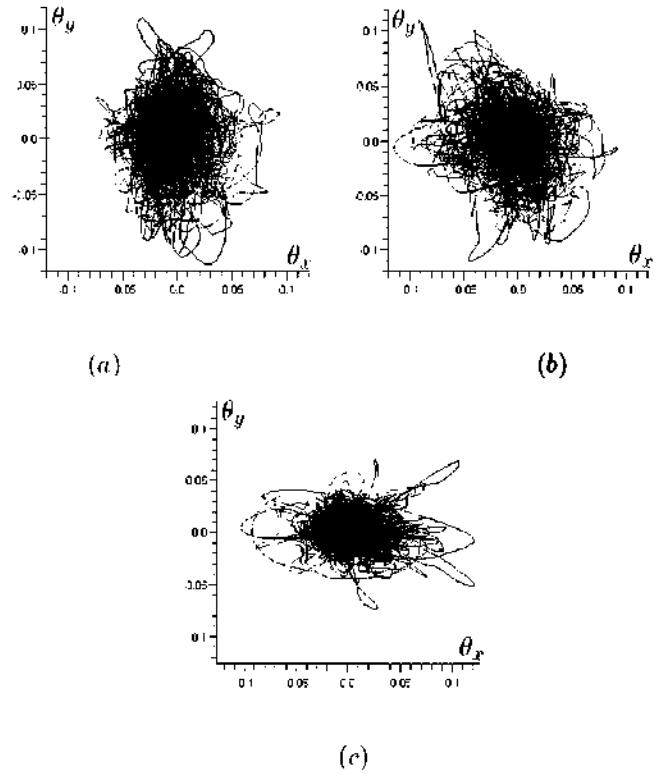

FIG. 5. Experimental data: (a) left-legged stance, (b) right-legged stance, and (c) two-legged stance.

set of experimental data (see Sec. II) and the contours of the basin of attraction that correspond to different depth z inside the basin (Sec. V B). From these curves a three-dimensional function is formed (see Sec. VI B) that models the basin of attraction of the particnlar experimental data set.

The desired cnrves are derived from the experimental data as follows. Let ns assnme that for modeling pnrposes, a cnrve is to be fit to the set of M experimental data points $\{x_i\}$, $i=1,\ldots,M$. Let us also assume that this curve is given by a function $\tilde{f}(x)$ that depends on K parameters α_i, $i=1,\ldots,K$, i.e., $\tilde{f}\equiv\tilde{f}(x,\alpha_1,\ldots,\alpha_K)$.

For the purposes of cnrve fitting, the sqnared distance χ^2 between the curve $\tilde{f}$ and the data points $\{x_i\}$,

$$\chi^2(x,\alpha_1,\ldots,\alpha_K)\equiv\sum_{i=1}^{M}[x_i-\tilde{f}(x_i,\alpha_1,\ldots,\alpha_K)]^2,$$

was considered as the cost function to be minimized.

The aim of the optimization was to calculate the (optimal) values of the control variables $\alpha_1,\ldots,\alpha_K$ that provide the cnrves of the desired form that best fit the data set (see Secs. V B and VI A below). For this reason, during each optimization process, the cost function of χ^2 was numerically minimized and the method nsed was the stochastic optimization method ALOPEX IV (see Sec. III B). Section III B gives a brief introdnction to the numerical stochastic optimization method of ALOPEX.

B. Brief introduction to ALOPEX stochastic optimization

The method of ALOPEX is a simple, yet very fast and efficient method of stochastic optimization.[38] It is an iterative procedure the main advantage of which being that no knowledge of the dynamics of the system or of the functional dependence of the cost function on the control variables is required.

In the present study we use the version ALOPEX IV of the method which calculates the value of the ith control variable in the $(k+1)$th iteration as follows:

$$\omega_i^{(k+1)}=\omega_i^{(k)}+c\Delta\omega_i^{(k)}\frac{\Delta f^{(k)}}{|\Delta f^{(k-1)}|}+g_i^{(k)},\quad i=1,\ldots,N,\quad (3)$$

where

- N is the number of the control variables,
- $\omega_i^{(k)}$ is the value of the ith control variable after the kth iteration,
- $f^{(k)}(\omega_1^{(k)},\omega_2^{(k)},\ldots,\omega_N^{(k)})$ is the value of the control function after the kth iteration,
- c is a constant with a value fixed at $c=0.4$ for the present study,
- $g_i^{(k)}$ is the stochastic element (random noise step),
- $\Delta\omega_i^{(k)}\equiv\omega_i^{(k)}-\omega_i^{(k-1)}$,
- $\Delta f^{(k)}\equiv f^{(k)}-f^{(k-1)}$, and
- $\Delta f^{(k-1)}\equiv f^{(k-1)}-f^{(k-2)}$.

For more information regarding ALOPEX stochastic optimization as well as applications of the method, see Refs. 3 and 38–42.

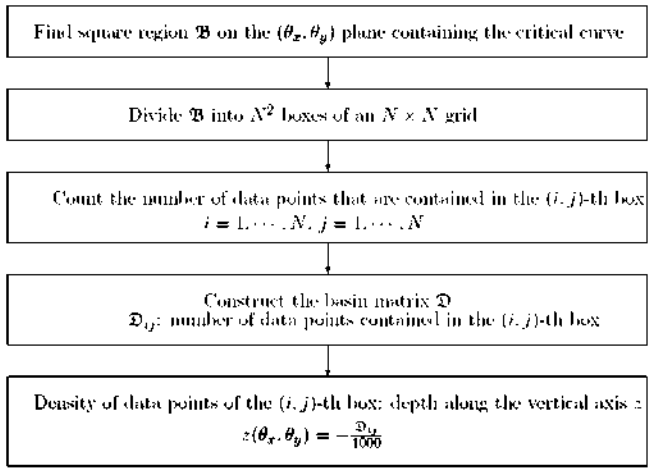

FIG. 6. Schematic representation of the calculation of the basin of attraction from experimental data.

IV. THE BASIN MATRIX $\mathfrak{D}$

A. Calculation of the basin matrix

For the calculation of the basin of attraction that is enclosed by the critical curve, the following procedure is followed (see Fig. 6):

(1) Consider $\theta_{\max}$ to be the maximum recorded valne of the angles that the snbject can lean to and still regain balance, as obtained from the experimental data (in absolnte terms) and a square region $\mathfrak{B}$ on the (θ_x,θ_y) plane containing the critical cnrve snch as

$$\mathfrak{B}=\{(\theta_x,\theta_y)\in\mathbb{R}^2|-|\theta_{\max}|\le\theta_x,\theta_y\le|\theta_{\max}|\}.$$

(2) Choose a scaling nnmber γ and divide the region $\mathfrak{B}$ into N^2 boxes of an $N\times N$ grid, where N is the integer part of $2\gamma|\theta_{\max}|+1$. The nnmber γ determines the resolntion of the grid of the basin of attraction and is chosen interactively: if γ is too small, fine details regarding the shape of the basin of attraction will be lost. On the other hand, large values of γ are limited by the number of experimental data points. It is assumed that the (i,j)th box of the grid corresponds to the point (θ_i,θ_j) of the (θ_x,θ_y) plane, in such a way that

$$\theta_i=\frac{|\theta_{\max}|}{N-1}(2i-N-1),\quad \theta_j=\frac{|\theta_{\max}|}{N-1}(2j-N-1).$$

(3) For each one of the three experiments (one for the two-legged and two for the one-legged stance) collect all five sets of reeorded experimental data that correspond to successful attempts to regain balance and count the number of data points that are contained in the (i,j)th box of the grid, where $i=1,\ldots,N$ and $j=1,\ldots,N$. This number gives the density of data points that are contained in the (i,j)th box of the grid, or in other words defines the depth of the (i,j)th box.

(4) Construct the $N\times N$ matrix $\mathfrak{D}$, the value of the element $\mathfrak{D}_{ij}$ of which gives the number of recorded data points that are contained in the (i,j)th box, as described above.

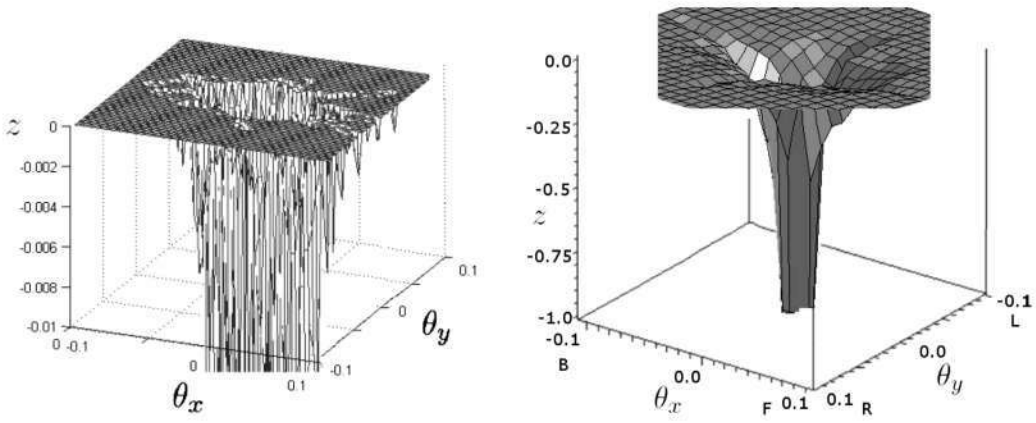

(a) (b)

FIG. 7. Three-dimensional representation of the basin of attraction as calculated from data density, $-|\theta_{\max}| \le \theta_x, \theta_y \le |\theta_{\max}|$. (a) Detail ($-0.01 \le z \le 0.0$) showing how the $N \times N$ grid is overlaid on the data points. (b) Drawing of the basin obtained from the data set ($-1.000 \le z \le -0.003$). The numerical values are $\theta_{\max}=0.1214$, dimension of the basin matrix is $\mathfrak{D}$:$N=65$, and the letters F, B, R, and L correspond to the four principal directions (forward, backward, right, and left, respectively).

The matrix $\mathfrak{D}$ gives a representation of the basin of attraction in terms of data density (number of recorded points).

B. Three-dimensional representation of the basin matrix

Let us now consider that the density of the recorded data points of the (i,j)th box of the grid corresponds to the depth of this box along the vertical axis z, as mentioned before. Then the basin of attraction that corresponds to the vertical stance and is enclosed by the critical curve can be visualized in three dimensions. In such a plot, the vertical (z) axis corresponds to data density as follows.

- The plane $z=0$ corresponds to the boundary of the basin of attraction (i.e., the critical curve).
- As the data density increases toward the attracting fixed point at vertical position, the values of z become more negative, the most negative z value corresponding to the attractor inside the basin.
- The values of the elements $\mathfrak{D}_{ij}$ take values from 0 to very large numbers; for this reason, these values have been divided, for the purposes of the present study, by 1000. This way the relation between depth $z(\theta_x, \theta_y)$ and data density $\mathfrak{D}_{ij}$ is $\forall\ i=i,\ldots,N$ and $\forall\ j=i,\ldots,N$,

$$z(\theta_x, \theta_y) = -\frac{\mathfrak{D}_{ij}}{1000}.$$

- All points that lie on the region $z \le -1.0$ of the basin of attraction (that corresponds to experimental data density of $\mathfrak{D}_{ij} > 1000$) are considered to belong to the attracting fixed point at (0,0) due to

(1) experimental error and
(2) effects of body sway (see Sec. I).

Figure 7 shows, as an example, the three-dimensional representation of the basin matrix $\mathfrak{D}$ as calculated from the experimental data of the two-legged stance that are shown in Fig. 5(c) using the procedure described above. For the calculation of the basin matrix $\mathfrak{D}$ shown in this figure, the best value of γ was found, by trial and error, to be equal to $\gamma=270$. From the experimental data of Fig. 5(c) there is $\theta_{\max}=0.1214$ (rads) and therefore $N=65$.

V. CALCULATION OF THE CONTOURS OF THE BASIN OF ATTRACTION

A. Graphical representation

For the purpose of calculating a number of m contours of the basin of attraction, based on the experimental data, m characteristic values of "depth" z are selected. Then, using an appropriate algorithm, the boundary of the region of the phase space of (θ_x, θ_y) for which the depth of the basin of attraction is more negative than the selected value z was numerically calculated. As an example, we present below $m=6$ contours that correspond to the depths $z=0$ (critical curve), $z=-0.003$, $z=-0.013$, $z=-0.100$, $z=-0.400$, and $z=-1.000$.

Figures 8(a)–8(c) present the calculated contours of the basin of attraction for the left-legged, the right-legged, and the two-legged stances, respectively, as were numerically calculated. As can be seen there are asymmetries and differences in the shape of the contours, as the depth z of the basin of attraction increases and also regarding different sides of the body (differences between left-legged and right-legged stances, or the two-legged stance).

B. Contour modeling

In Secs. V B and VI we consider the phase space of the two angles on a polar coordinate system (ρ, θ) instead of the Cartesian (θ_x, θ_y), such that $\rho \equiv \sqrt{\theta_x^2 + \theta_y^2}$, $\rho \ge 0$ and $\theta \equiv \arctan(\theta_y/\theta_x)$, $\theta = 0, \ldots, 2\pi$.

To model the contours of the basin of attraction that cut the basin of attraction at different depths z, we consider that each contour is represented by a closed curve on the (θ_x, θ_y)

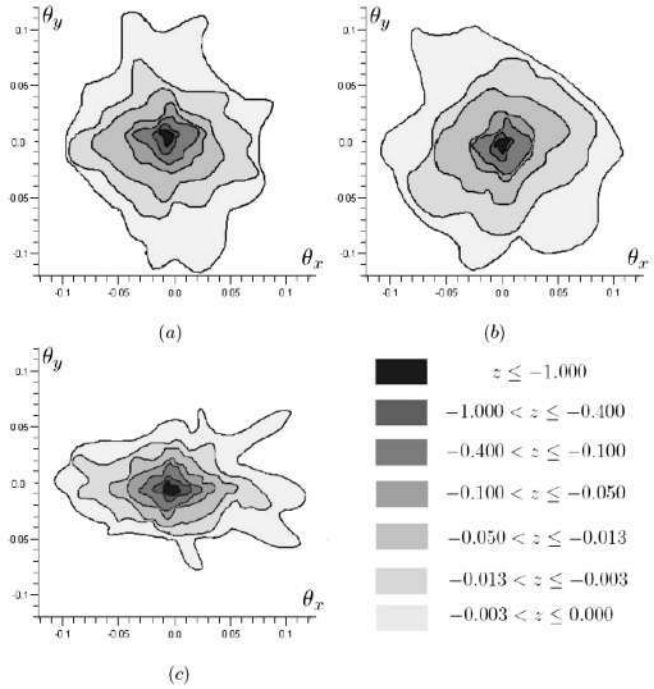

FIG. 8. Contours of the basin matrix $\mathfrak{D}$ corresponding to different depths z: (a) left-legged stance, (b) right-legged stance, and (c) two-legged stance.

plane. During the present study a number of functions that can possibly represent such curves have been considered. The aim was to find a function that provides closed curves in polar coordinates that will allow full control of the observed oscillations of the contours. The curve that models each contour of the basin of attraction should enclose all data points that have been calculated to lie deeper within the basin than the depth z that characterizes the particular contour.

After an extensive study of families of functions with the above properties we concluded that the best choice is a function which includes an expansion of sines and cosines of the following form:

$$\rho(\theta) = a\left[1 + \sum_{k=1}^{n_z} a_k \cos(k\theta) + \sum_{k=1}^{n_z} b_k \sin(k\theta)\right]^{-1}, \tag{4}$$

where for each constant depth z the parameters a, a_k, and b_k take real values and the number $n_z \in \mathbb{N}^\star$ depends on z and gives the number of harmonics that best fit the experimental data. The values of n_z were chosen for each contour by trial and error.

For the curves representing the contours given by Eq. (4) to be closed curves, the values of the parameters a_k and b_k have to be chosen appropriately. This is not a problem, however, as the values of these parameters are chosen in the present study so as to provide the curves that best fit the experimental data, and are forced by the optimization algorithm to create closed curves.

Tables 1 and 2 (Ref. 43) present, as an example, the parameters that give the closed curves that best describe the contours of the two-legged experiment and that are shown in Fig. 8(c). For the calculation of the contours, the ALOPEX IV optimization algorithm was used to optimize a χ^2 fit (see Sec. I). For a detailed description of the computational procedure of curve fitting using ALOPEX optimization, see Ref. 3.

VI. MODELING THE THREE-DIMENSIONAL BASIN OF ATTRACTION

A. The functional dependence of the parameters on depth z

As can be observed in Tables 1 and 2,[43] for a given depth z and a given number of harmonics n_z, the parameters a, a_k, and b_k $(k=1,\ldots,n)$ that control the shape of the contours for the particular z, as described by Eq. (4), are dependent on z. In other words they can be considered to be functions of z and therefore Eq. (4) can be rewritten in the form

$$\rho(\theta,z) = a(z)\left[1 + \sum_{k=1}^{n_z} a_k(z)\cos(k\theta) + \sum_{k=1}^{n_z} b_k(z)\sin(k\theta)\right]^{-1}. \tag{5}$$

To model the functional dependence of the parameters a, a_k, and b_k $(k=1,\ldots,n)$ on z, we have concluded, by numerical observation, that a sum of Gaussian functions of the form described in Eq. (6) that follows models the numerically calculated values in a highly satisfactory way,

$$\begin{aligned} a(z) &= \sum_{i=1}^{m} c_i e^{-p_i(z-q_i)^2}, \\ a_k(z) &= \sum_{i=1}^{m^{ak}} c_i^{ak} e^{-p_i^{ak}(z-q_i^{ak})^2}, \\ b_k(z) &= \sum_{i=1}^{m^{bk}} c_i^{bk} e^{-p_i^{bk}(z-q_i^{bk})^2}. \end{aligned} \tag{6}$$

In Eq. (6) above, $m, m^{ak}, m^{bk} \in \mathbb{N}^\star$ denote the number of Gaussian functions used to best fit the dependence of the calculated values of the parameters a, a_k, and b_k $(k=1,\ldots,n_z)$ on z, respectively (found by trial and error). The real parameters c_i, p_i, q_i, $i=1,\ldots,m$, c_i^{ak}, p_i^{ak}, q_i^{ak}, $i=1,\ldots,m^{ak}$ and c_i^{bk}, p_i^{bk}, q_i^{bk}, $i=1,\ldots,m^{bk}$ are parameters of the fit.

As mentioned in Sec. V, for the numerical best fit of functions of the type (6) to the data of Tables 1 and 2,[43] the ALOPEX IV optimization algorithm was implemented for a χ^2 fitting of the curves. In Tables 3–6 (Ref. 43) we present, as an example, the parameters that best fit the values of a, a_k, and b_k that are shown in Tables 1 and 2.[43]

B. A model of the basin of attraction as a three-dimensional function

By summarizing and combining the conclusions and best fits presented in Secs. IV, V, and VI A, we conclude that the basin of attraction that is bound by the critical curve (as described in Sec. I) and includes the spiral sink that models the vertical "quiet" stance (within the limits of body sway, see Sec. I) can be given in a three-dimensional system of cylindrical coordinates (ρ,θ,z) by a function of the form

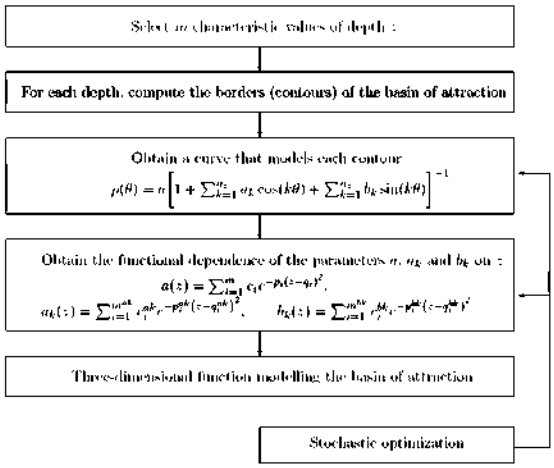

FIG. 9. Schematic representation of the process of modeling the basin of attraction as a three-dimensional function.

$$\rho(\theta,z) = \left[\sum_{i=1}^{m} c_i e^{-p_i(z-q_i)^2}\right] \times \left\{1 + \sum_{k=1}^{n_z}\left[\sum_{i=1}^{m^{ak}} c_i^{ak} e^{-p_i^{ak}(z-q_i^{ak})^2}\right]\cos(k\theta) + \sum_{k=1}^{n_z}\left[\sum_{i=1}^{m^{bk}} c_i^{bk} e^{-p_i^{bk}(z-q_i^{bk})^2}\right]\sin(k\theta)\right\}^{-1}, \quad (7)$$

where $n_z, m, m^{ak}, m^{bk} \in \mathbb{N}^*$, $\theta = 0, \ldots, 2\pi$, and $c_i, p_i, q_i, c_i^{ak}, p_i^{ak}, q_i^{ak}, c_i^{bk}, p_i^{bk}, q_i^{bk} \in \mathbb{R}$.

The variable z that represents the depth of the basin is considered due to experimental error as well as the effects of body sway (see also Secs. I, IV, and VI) to take values $z=-1, \ldots, 0$, where $z=0$ corresponds to the critical curve, which is the boundary of the basin of attraction, and $z=-1$ corresponds to the attractor of vertical stance.

In Fig. 9 a schematic representation of the modeling process is shown. Figure 10 presents, as an example, a plot of the calculated three-dimensional function of the basin of attraction that corresponds to the two-legged stance experiment. The values of the parameters are given in Tables 1–6.[43]

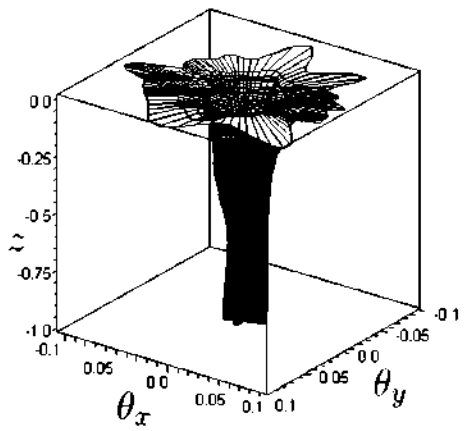

FIG. 10. The basin of attraction, as given by Eq. (7), and the parameter values of Tables 1–6 (Ref. 43). The function of the basin of attraction is shown for $-|\theta_{max}| \le \theta_x, \theta_y \le |\theta_{max}|$ and $-1.000 \le z \le -0.003$.

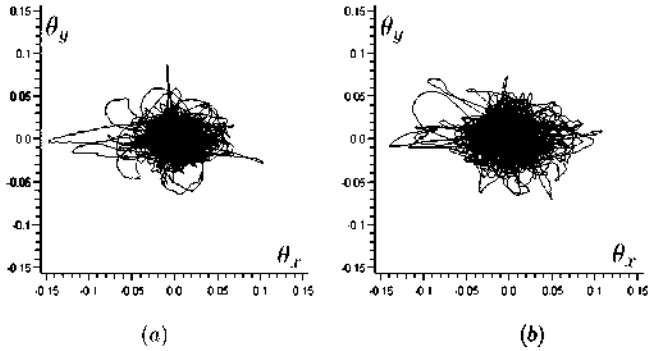

FIG. 11. Experimental data, two-legged stance, for the second subject (a) data set 1 and (b) data set 2.

VII. A TEST OF THE SENSITIVITY OF THE METHOD TO DIFFERENT DATA SETS

To further examine the robustness of our method, additional data from a different subject (a 30-year-old healthy male who was not an athlete) have been collected. Protocol 1 (two-legged stance) has been followed, as described in Sec. II, this time twice. Care was taken to minimize the time between the two successive data collection sessions so as to avoid any possible effect of training and/or change in physical condition on the movement patterns of the subject. The set of the recorded data of the five successful attempts, plotted on the phase space of (θ_x, θ_y), is shown in Fig. 11.

For the data shown in Fig. 11 we comment the following:

- Small changes can be observed in the shape of the region that defines the boundary of the basin of attraction and thus the critical curve (i.e., the curve enclosing all data points: all possible angles the subject can lean to and still regain balance).
- The overall shape and, more importantly, the size of the critical curve is the same for both data sets of the two different data collection sessions.
- For both data sets the same value of θ_{max} was calculated: $\theta_{max}=0.1401$.
- The region of highest density of trajectories (i.e., the blackest region) appears to remain the same for both data sets.

Figure 12 shows a detail of the data sets plotted in three dimensions. In these graphs the similarity of the two different data sets becomes more obvious: apart from the small changes in the shape of the boundary at $z=0$, the overall shape and details of the plotted basin of attraction can be observed to be the same for both plots.

To examine the similarity of the data sets in more detail, the contours of the basin of attraction were calculated, following the exact procedure described in Sec. V. Figure 13 shows the results. As can be observed in Fig. 13, apart from the exception of the critical curve (contour for $z=0$), there is no significant difference between the calculated contours of

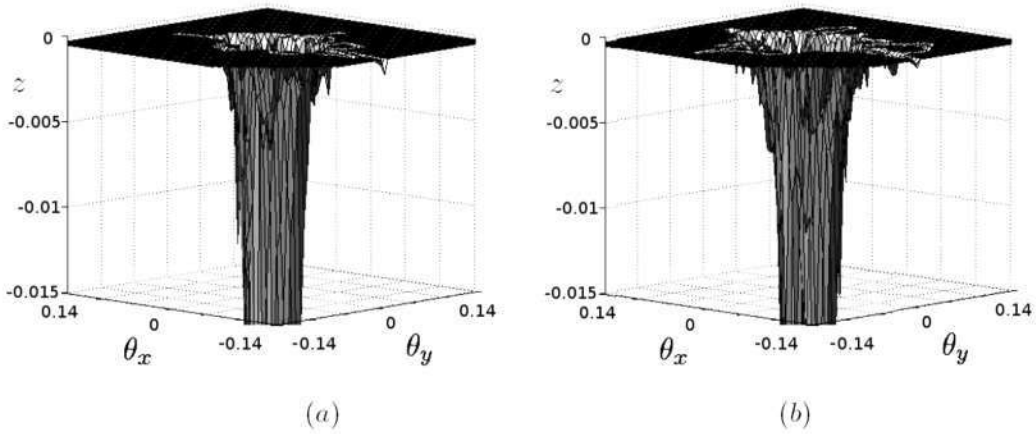

FIG. 12. Showing a detail ($-0.015 \leq z \leq 0$) of the three-dimensional representation of the basin of attraction as calculated from data density, $-|\theta_{\max}| \leq \theta_x, \theta_y \leq |\theta_{\max}|$. The data correspond to the second subject (a) data set 1 and (b) data set 2. The numerical values are $\theta_{\max}=0.1401$, dimension of the basin matrix is $\mathfrak{D}: N=65$.

the basin of attraction of the second subject for the two different data sets. The overall shape and size of the contours are the same for both data sets, and the small differences observed were expected as a result of the unavoidable experimental error.

Figure 13 proves the robustness of our method: the calculated basin of attraction has been shown (through its contours) to have the same (or very similar within the limitations of experimental error) size and shape, even for two data sets that were collected during different experimental sessions. The same results would of course be obtained if these two data sets were combined, the only difference would have been in the details of the shape of the boundary of the basin (critical curve).

VIII. DISCUSSION AND CONCLUSIONS

We have presented a method of estimating the basin of attraction as a function in three dimensions on a cylindrical coordinate system, the coordinates of which are those of the phase space of our model and the axis z that corresponds to depth inside the basin. Our method has been applied to the problem of estimating the basin of attraction that includes the attractor of vertical quiet stance in a model of the process of regaining balance. For this reason, the experimentally recorded movement patterns of an elite decathlete, while trying to regain balance after perturbation from quiet stance, have been modeled and a three-dimensional function of the corresponding basin of attraction has been calculated. The robustness and sensitivity of the method to repeated analysis have been successfully tested by its application to two different data sets of a second subject.

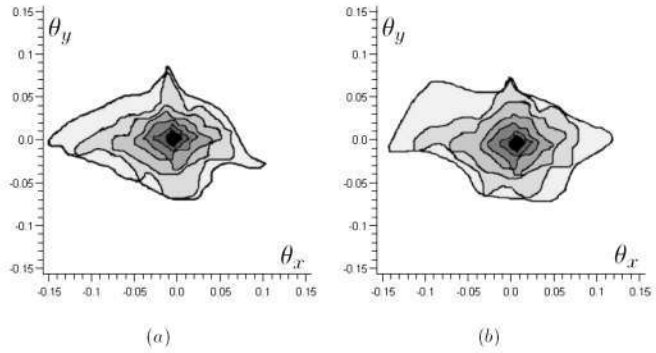

FIG. 13. Contours of the basin matrix $\mathfrak{D}$ of the second subject that correspond to different depths z: (a) data set 1 and (b) data set 2. The color index is the same as that of Fig. 8.

We have also shown how to obtain the contours of the basin of attraction. This has many uses in human balance, for understanding the difference between extreme and normal movements, as well as the subject's preferred movement patterns.

There are a number of assumptions underlying our method.

(1) The basin of attraction is static for the duration of an experimental trial (and possibly beyond).
(2) The amount of data collected (see Sec. II) is sufficient to compute the basin's shape.
(3) The local depth of the basin, and thus its shape, is reflected by the number of sample points found at a given location, i.e., the longer the system resides in a neighborhood, the deeper the basin there; and, consequently, the greater the difference between adjacent rectangles in terms of data points counted, the greater the slope of the basin wall at that location. This, in turn, has implications concerning the assumed strength of the attractor given by $\dot{x}=-dV/dx$, where V is the potential energy of the system.
(4) The change in basin heights is sufficiently smooth to fit an exponential function to it.

The novelty of the method presented here is that it goes beyond the statistical description of the experimental data, providing a function the describes the shape of the basin of attraction. This makes our model very powerful: based on the numerically estimated geometry and given appropriate initial conditions, one can generate synthetic dynamics and provide artificial data that simulate the experimentally obtained data from that particular subject.

Our method is not restricted to the study of human balance, but it has also many uses in a wide variety of applications, in which the basin of attraction is desired to be obtained from experimental data.

ACKNOWLEDGMENTS

This work was supported by Ingenio Mathematica (i-math) (Project No. C3-0106) as well as the programs Ramón y Cajal 2004 and I3 2006, Ministerio de Educación y Ciencia, Spain.

[1]J. R. Stirling and M. S. Zakynthinaki, Chaos **14**, 96 (2004).
[2]J. R. Stirling and M. S. Zakynthinaki, Lecture Notes of the ICB Seminar, Mechanical Loads of the Human Motor System—Injury Prevention, 2005, Vol. 64, p. 39 (unpublished).
[3]M. S. Zakynthinaki, J. R. Stirling, A. L. D. de Durana, C. A. C. Martínez, M. S. Quintana, and J. S. Molinuevo, Comput. Phys. Commun. **179**, 562 (2008).
[4]J. G. Milton, Chaos **19**, 026101 (2009).
[5]J. Milton, J. L. Cabrera, T. Ohira, S. Tajima, Y. Tonosaki, C. W. Eurich, and S. A. Campbell, Chaos **19**, 026110 (2009).
[6]L. H. Ting, K. W. van Antwerp, J. E. Scrivens, J. L. McKay, T. D. J. Welch, J. T. Bingham, and S. P. DeWeerth, Chaos **19**, 026111 (2009).
[7]B. G. Bardy and O. Oullier, J. Motor Behav. **39**, 326 (2007).
[8]N. Bernstein, *The Coordination and Regulation of Movement* (Pergamon, New York, 1967).
[9]B. G. Bardy, O. Oullier, R. J. Bootsma, and T. A. Stoffregen, J. Exp. Psychol. Hum. Percept. Perform. **28**, 499 (2002).
[10]B. A. Kay, Hum. Mov. Sci. **7**, 343 (1988).
[11]L. M. Nashner, Exp. Brain Res. **26**, 59 (1976).
[12]L. M. Nashner and G. McCollum, Behav. Brain Sci. **8**, 135 (1985).
[13]M. Lauk, C. C. Chow, A. E. Pavlik, and J. J. Collins, Phys. Rev. Lett. **80**, 413 (1998).
[14]E. T. Hsiao-Wecksler, K. Katdarea, J. Matsona, W. Liua, L. A. Lipsitzc, and J. J. Collins, J. Biomech. **36**, 1327 (2003).
[15]G. E. Riccio and T. A. Stoffregen, Hum. Mov. Sci. **7**, 265 (1988).
[16]S. Yoneda and K. Tokumasu, Acta Oto-Laryngol. **102**, 87 (1986).
[17]J. J. Collins and C. J. DeLuca, Phys. Rev. Lett. **73**, 764 (1994).
[18]B. G. Bardy, L. Marin, T. A. Stoffregen, and R. J. Bootsma, J. Exp. Psychol. Hum. Percept. Perform. **25**, 1284 (1999).
[19]G. McCollum and T. K. Leen, J. Motor Behav. **21**, 225 (1989).
[20]A. Levin, IEEE Trans. Autom. Control **39**, 2471 (1994).
[21]J. R. Cusumano and B. W. Kimble, Nonlinear Dyn. **8**, 213 (1995).
[22]M. T. R. Genesio and A. Vicino, IEEE Trans. Autom. Control **30**, 747 (1985).
[23]H. A. Antosiewicz, *A Survey of Lyapunov's Second Method*, Contributions to the Theory of Nonlinear Oscillations Vol. 4 (Princeton University Press, Princeton, 1958), pp. 141–166.
[24]W. Hahn, *Theory and Applications of Lyapunov's Direct Method* (Prentice-Hall, Englewood Cliffs, 1963).
[25]J. P. L. Salle and S. Lefschetz, *Stability by Lyapunov's Direct Method* (Academic, New York, 1961).
[26]A. M. Letov, *Stability in Nonlinear Control Systems* (Princeton University Press, Princeton, 1961).
[27]D. D. Perlmutter, *Stability of Chemical Reactors* (Prentice-Hall, Englewood Cliffs, 1972).
[28]J. R. Hewit and C. Storey, Electron. Lett. **2**, 408 (1966).
[29]W. O. Paradis and D. D. Perlmutter, AIChE J. **12**, 13 (1966).
[30]E. J. Davison and K. C. Cowan, Int. J. Control **9**, 349 (1969).
[31]J. Texter, IEEE Trans. Autom. Control **19**, 62 (1974).
[32]J. A. Y. C. Grebogi and E. Ott, Phys. Rev. Lett. **56**, 1011 (1986).
[33]A. I. Lebedev and I. Sluchinskaya, Crystallogr. Rep. **49**, 594 (2004).
[34]H. Urai, IEEE Trans. Magn. **21**, 2676 (1985).
[35]A. L. Schwab and M. Wisse, Proceedings of DETC'01. ASME 2001 Design Engineering Technical Conferences and Computers and Information in Engineering Conference, 2001, pp. 1–9 (unpublished).
[36]K. Pakdaman, C. Grotta-Ragazzo, C. P. Malta, O. Arino, and J.-F. Vibert, Neural Networks **11**, 509 (1998).
[37]J. R. Stirling, C. A. C. Martínez, A. L. D. de Durana, and M. S. Quintana, "Analysis of inbalance in elite sport with application to improvement of technique and injury prevention," Consejo Superior de Deportes Technical Report No. 07/UPB10/07, 2007.
[38]M. S. Zakynthinaki, "Stochastic optimization for adaptive correction of atmospheric distortion in astronomical observation," Ph.D. thesis, Technical University of Crete, 2001.
[39]M. S. Zakynthinaki and Y. G. Saridakis, Comput. Phys. Commun. **150**, 274 (2003).
[40]M. S. Zakynthinaki and J. R. Stirling, Comput. Phys. Commun. **176**, 98 (2007).
[41]J. R. Stirling, M. S. Zakynthinaki, and V. Billat, Bull. Math. Biol. **70**, 1348 (2008).
[42]M. S. Zakynthinaki and J. R. Stirling, Comput. Phys. Commun. **179**, 888 (2008).
[43]See supplementary material at http://dx.doi.org/10.1063/1.3337690 for Tables 1–6.